J Mol Model (2011) 17:465–475
DOI 10.1007/s00894-010-0734-4

ORIGINAL PAPER

Antitumor activity of bent metallocenes: electronic structure analysis using DFT computations

Dhurairajan Senthilnathan · Sundararajan Vaideeswaran · Ponnambalam Venuvanalingam · Gernot Frenking

Received: 9 February 2010 / Accepted: 26 April 2010 / Published online: 22 May 2010

Abstract The antitumor activities of bent metallocenes $[Cp–M–Cp]^{2+}$ (M = Ti, V, Nb, Mo) and complexes of them with guanine, adenine, thymine and cytosine nucleotides have been probed using electronic structure calculations. DFT/BP86 calculations have revealed that the bent metallocene–nucleotide interaction strongly depends on the stability of the hydrolyzed form of the bent metallocene dichloride $[Cp_2M]^{2+}$ species, and in turn the stability of the $[Cp_2M]^{2+}$ species strongly depends on the electronic structure of $[Cp_2M]^{2+}$. Detailed electronic structure and Walsh energy analyses have been carried out for the hydrolyzed forms of four $[Cp–M–Cp]^{2+}$ (M = Ti, V, Nb, Mo) species to find out why the bent structure is unusually stable. Energy changes that occur during the bending process in frontier molecular orbitals as well as the $p(\pi)$–$d(\pi)$ overlap have been invoked to account for the anticipated antitumor activities of these species. The bonding situation and the interactions in bent metallocene–nucleotide adducts were elucidated by fragment analysis. Of the four nucleotides complexed with the four bent metallocenes, adenine and guanine show better binding abilities than the other two nucleotides. Metallocenes of second-row transition metals exhibit better binding with pyrimidine-base nucleotides. In particular, the Lewis acidic bent metallocenes interact strongly with nucleotides. The antitumor activity is directly related to the binding strength of the bent metallocene with nucleotide adducts, and the computed interaction energy values correlate very well with the experimentally observed antitumor activities.

Keywords Bent metallocenes · Antitumor activity · Energy decomposition analysis · Nucleotides · Density functional theory (DFT)

D. Senthilnathan · S. Vaideeswaran · P. Venuvanalingam (✉)
School of Chemistry, Bharathidasan University,
Tiruchirappalli 620024, India
e-mail: venuvanalingam@yahoo.com

G. Frenking
Fachbereich Chemie, Philipps Universität,
35032 Marburg, Germany

Introduction

Cancer has emerged as a major public health problem in developing countries, as well as in industrialized nations. According to the *World Cancer Report*, cancer rates could increase by a further 50% to 15 million new cases by the year 2020. Chemists are attempting to synthesize new drugs that will not only eradicate tumors, but when used in combination with other agents, may turn many cases of rapidly fatal cancer into "manageable" chronic illnesses. One notable group of compounds that have been investigated as anticancer drugs are the bent metallocenes.

Under physiological conditions, bent metallocene dihalides (Cp_2MX_2; X = halogens) undergo rapid and extensive hydrolysis similar to that of *cis*-platin, and at low pH they exist as $[Cp_2M]^{2+}$, which possesses a bent structure [1]. In this form, they show a high degree of similarity to *cis*-platin in terms of structure and binding properties. This has led to the speculation that metallocene drugs utilize DNA as their primary biological target, and that they bind with DNA in a similar manner to *cis*-platin [1, 2].

Bent metallocene dihalides (Cp_2MX_2; Cp = η^5-C_5H_5; M = Ti, V, Nb, Mo; X = F, Cl, Br, I, NCS and N_3) are highly active against numerous tumor cell lines, so a variety of antitumor-active bent metallocene–nucleotide complexes have been synthesized and reported [1]. The antitumor activities of these

complexes have been studied extensively [1–20]. The vastly different chemical stabilities of each of these metallocenes at physiological pH and their different coordination chemistries point to significantly different mechanisms of antitumor action for each metallocene [21–27]. There is some evidence for the interaction of vanadocene dichloride with DNA in vivo [28], but there is a lack of structural information on such DNA complexes. At the same time, the interactions of four bent metallocenes with DNA nucleotides have been reported, and these species have been structurally characterized [1].

Titanocene dichloride is the only metallocene that is in clinical trials, and further work aimed at checking its suitability for use as a drug for cancer treatment is in progress. The poor stability of this drug at pH 6–7 is one of the issues that has slowed the development of a suitable formulation for administration and the design of titanocene-based drugs with improved activity.

The stability of $[Cp_2M]^{2+}$ very much depends on the electronic configuration of the metal [29, 30]. The bonding in normal metallocenes has been investigated and reported in numerous theoretical and experimental papers [31–34]. Therefore, it is interesting to consider how the bending conformation affects their electronic structures, which in turn influence their stability, reactivity and drug action.

In normal metallocenes, the π orbitals of two parallel $C_5H_5^-$ ligands which have D_5d geometry yield three sets of approximately degenerate orbitals: a low-lying filled pair of a_{1g} and a_{2u} symmetry, a set of filled orbitals, e_{1g} and e_{1u}, and a high-lying set of empty antibonding orbitals of symmetry e_{2g} and e_{2u}. These interact with metal orbitals such as e_{1g} (d_{xz}, d_{yz}), e_{2g} ($d_{x^2-y^2}$, d_{xy}) and a_{1g} (d_{z^2}). In the complex, there are strong interactions with metal *s* and *p* orbitals as well as with the e_{1g} set. The remaining three *d* orbitals of the metal, the a_{1g} and the e_{2g} set, remain essentially nonbonding. Thus, the *d*-level splitting is $e_{2g} \leq a_{1g} < e_{1g}$. When normal metallocenes are bent, the orbitals of the e_{1g} set are stabilized and those from the a_{1g} and e_{2g} sets are destabilized. This destabilization is due to the increased σ antibonding upon bending. Further, the stabilizing/destabilizing nature of the orbitals depends largely on the metal ion, the oxidation state of the metal, and the bending angle. It has been noted that certain metal ions in specific oxidation states prefer bent conformations. Though Hoffmann et al. [29, 30] and Bercaw et al. [35] have tried to qualitatively explain the bent shapes of certain metallocenes, a quantitative investigation of this in relation to the reactivity of bent metallocenes is still awaited.

In the work reported in this paper, the electronic structures of bent metallocenes and their antitumor activities were explored using density functional theory at the BP86 level. The changes in the electronic structures of antitumor-active metallocenes with respect to the bending process were derived using electronic structure analysis. The stabilities of $[Cp_2M]^{2+}$ (M = Ti, V, Nb, Mo) species were correlated with their nucleotide interactions. Further, the bonding situation in bent metallocene–nucleotide complexes was examined using fragment analysis and available experimental crystal structure information. This provides some useful insights into the mechanism of antitumor action of these bent metallocenes.

Computational details

All density-functional calculations were carried out using the Amsterdam density functional (ADF 2007) package [36–38]. A generalized gradient approximation (GGA) functional consisting of Becke's exchange and correlation expression proposed by Perdew, Burke, and Ernzerhof [39] was utilized. Basis sets of triple-ζ and one polarization function (TZP) were employed. Relativistic effects were included by means of the zero-order regular approximation (ZORA) [40–42]. Metallocene–nucleotide bonding interactions were analyzed with the energy decomposition scheme of the ADF program, which is based on the EDA method of Morokuma [43] and the ETS method of Ziegler [44]. The instantaneous interaction energy ΔE_{int} can be divided into three components:

$$\Delta E_{int} = \Delta E_{elstat} + \Delta E_{Pauli} + \Delta E_{orb}$$

ΔE_{elstat} gives the electrostatic interaction energy between the fragments, which is calculated with the frozen electron-density distribution in the geometry of the complex. This can be used as an estimate of the electrostatic contribution to the bonding interactions. The second term in the above equation, ΔE_{Pauli}, gives the repulsive orbital interaction between occupied orbitals of the two fragments due to antisymmetrization. The last term gives the stabilizing orbital interactions, ΔE_{orb}, which can be considered to be an estimate of the covalent contribution to the bonding. Thus, the ratio $\Delta E_{elstat}/\Delta E_{orb}$ may be used to describe the relative electrostatic/covalent character of the bond [45–47]. Frenking and coworkers [48–51] have reviewed the use of EDA analysis to understand chemical bonding in many classes of chemical compounds.

Results and discussion

The geometries of the bent metallocene species $[Cp_2M]^{2+}$ (M = Ti, V, Nb, Mo) were optimized at the BP86/TZP level, and all of them were found to have bent geometries. The bending angle (*Y*) and other important parameters of the ions are listed in Table 1. To examine the effect of the degree of bending on the total and various orbital energies, the bent

Table 1 Bending angles (Y), angle φ(Cp–M–Cp), bond distances ($d_{Cp'–M}$), and out-of-plane bending angles (θ) of the ring hydrogens in the optimized geometries of $[Cp_2M]^{2+}$ species at the BP86/TZP level

	Y	φ (Cp-M-Cp)	$d_{Cp'-M}$	θ
$[Cp_2Ti]^{2+}$	26.7	126.6	2.0	2.6
$[Cp_2V]^{2+}$	43.4	93.2	2.2	0.9
$[Cp_2Nb]^{2+}$	44.8	90.4	2.1	0.9
$[Cp_2Mo]^{2+}$	39.5	101.0	2.0	1.1

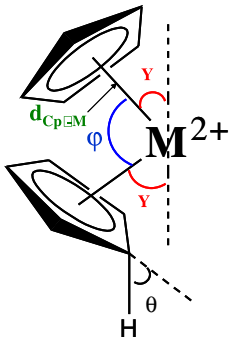

Angle Y $\left(Y = \frac{180 - \varphi}{2}\right)$ and θ in degrees and bond length in Å, M = Ti, V, Nb, Mo

metallocenes $[Cp_2M]^{2+}$ were optimized at fixed Cp–M–Cp angles; calculations were performed every 10° in the interval 120–180°. The variation of the total energy of the system with bending angle is presented in Fig. 1. This clearly shows that the bent shape is more stable than the linear one for $[Cp_2M]^{2+}$ (M = Ti, V, Nb, Mo). The most stable bending angles for the four metallocenes range from 135.2° to 153.3°. The frontier molecular (FMO) orbital energies for the minimum energy structures of $[Cp_2M]^{2+}$ (M = Ti, V, Nb, Mo) are presented in Table 2.

The basic trend for all of the systems is for the frontier molecular orbitals to become much closer during bending compared to those in normal metallocenes, and this leads to the unusual reactivity of these species. The molecular orbitals descending from the e_{1g} set are stabilized upon bending, while those descending from a_{1g} and e_{2g} are destabilized. For the lower orbitals, $1a_1$, b_2 and $2a_1$, this trend is the result of increased σ antibonding as the Cp–M–Cp angle changes from 180° [18]. According to the literature [29, 30], the order of stability with respect to molecular orbitals of bent metallocenes will be: bonding orbitals ($1a_1 > b_2 > 2a_1$) > antibonding orbitals ($b_1 > a_2$). The FMO energies for the four metallocenes (Table 2) clearly reflect the above trend. From a symmetry point of view, the bent metallocenes extend their coordination tetrahedrally, where the b_2 and $2a_1$ MOs are involved in bond formation with the incoming ligand orbitals. The bending process destabilizes the bonding $2a_1$ molecular orbital and stabilizes the antibonding b_1 molecular orbital. Hence, the reactivity of the bent metallocene depends on the energy gap between the higher-lying bonding molecular orbital ($2a_1$) and the lower-energy antibonding molecular orbital (b_1). This is well reflected in the values listed in Table 2. Based on the energy difference between the $2a_1$ and b_1 orbitals, the order of reactivity for the four metallocenes is: $[Cp_2V]^{2+} > [Cp_2Nb]^{2+} > [Cp_2Mo]^{2+} > [Cp_2Ti]^{2+}$.

The optimized geometry of titanocene $[Cp_2Ti]^{2+}$ shows a bending angle Y of 26.7°, which is due to the lack of nonbonding electrons ($1a_1$) in the metal to repel the electrons of the Cp ring. The distance between the metal and the Cp ring ($d_{Cp'–M}$) is 2.0 Å. The $[Cp_2Ti]^{2+}$ species has the smallest bending angle (26.7°) of the metallocenes, leading to the largest energy gap (2.06 eV) between the $2a_1$ and b_1 orbitals. The complexes $[Cp_2V]^{2+}$ and $[Cp_2Nb]^{2+}$ have larger bending angles of 43.4° and 44.8°, respectively, and this leads to the smallest energy gap between the MOs $2a_1$ and b_1. A comparison of $[Cp_2Ti]^{2+}$ with $[Cp_2V]^{2+}$ shows that the larger bending angle in the latter is due to the repulsion between the nonbonding electron (d^1) and the bond electron in the M–Cp molecular orbitals. However, $[Cp_2Mo]^{2+}$ is less bent than $[Cp_2Ti]^{2+}$ and $[Cp_2V]^{2+}$ because of the larger size of Mo(IV) than all of the other M(IV) ions considered here. The large size of the metal means that it will effectively overlap with the Cp^- ring even though it experiences high repulsion from the nonbonding electrons. Another interesting observation (Table 1) is that the H atoms attached to the Cp-ring carbons are bent out of the plane (outward) of the Cp ring. A detailed theoretical study performed by Schleyer et al. [52] concluded that the bending occurs in the outward direction when the central metal atom is bonded to a small ring and has highly diffuse orbitals, while the bending occurs in the inward direction when the central metal atom is bonded to a large ring and has less diffuse orbitals. In the antitumor-active bent metallocenes considered here, the Cp^- ring protons show outward bending due to the effective overlap of highly diffuse empty *d* orbitals with the Cp^- ring. The outward bending angle θ depends on the effective overlap of the *d* orbital of M(IV) with the filled $p(\pi)$ orbital of the Cp ring

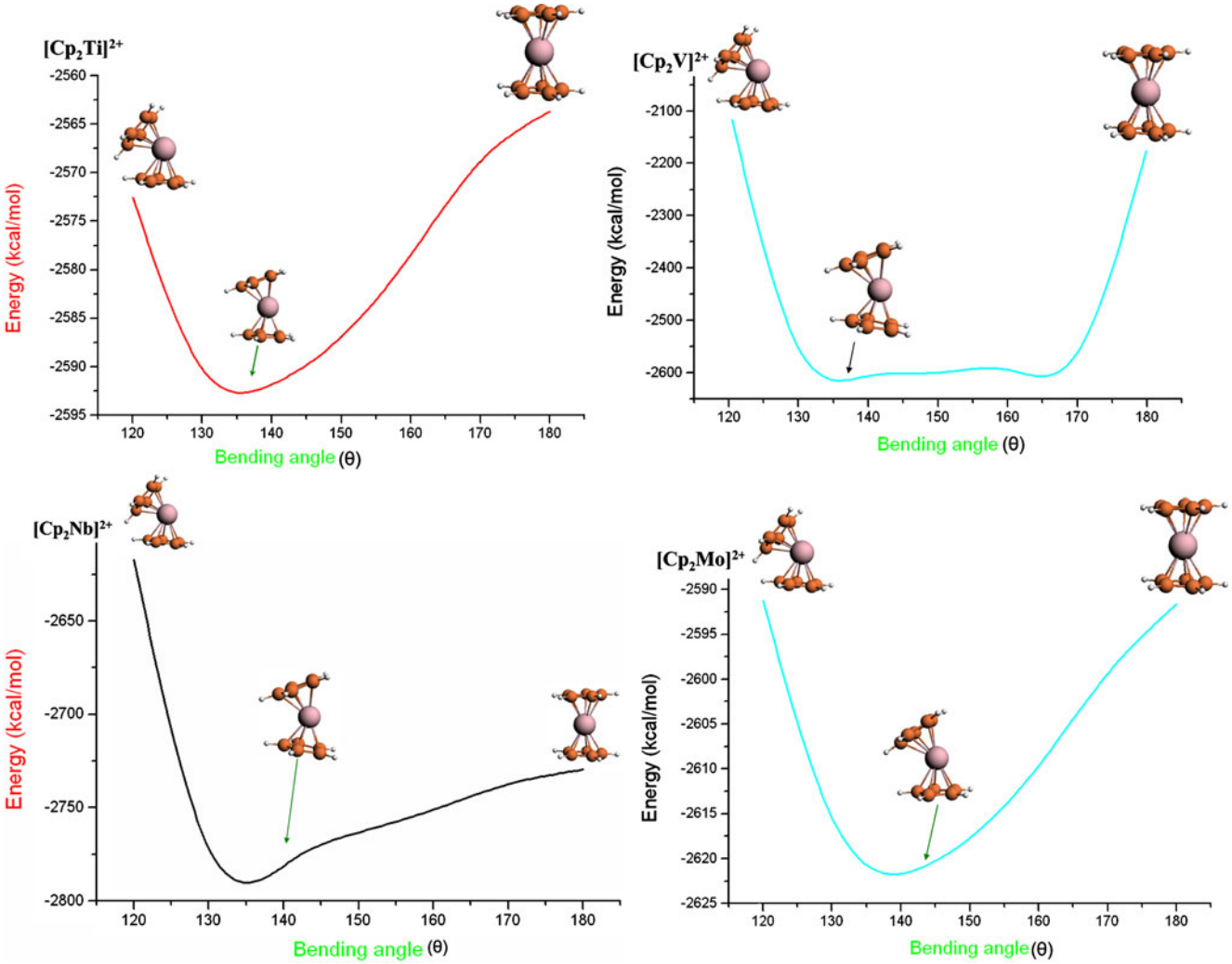

Fig. 1 Bending energy profiles for $[Cp_2M]^{2+}$ (M = Ti, V, Nb, Mo)

and their symmetries. The minimal value of φ(Cp–Ti–Cp) leads to the maximal outward bending of the Cp-ring hydrogens (θ). The minimal bending of the Cp ring from the normal 180° plane allows the effective overlap of the p (π) orbital of Cp with the d(π) orbital of the metal for p(π)–d(π) bond formation. The effective overlap of the p(π) and d(π) orbitals directly reflect the maximal outward bending of the ring hydrogens. This trend is clearly observed and listed in Table 1.

Table 2 BP86/TZP frontier molecular orbital energies (eV) for the minimum energy structures of $[Cp_2M]^{2+}$ (M = Ti, V, Nb and Mo) species

	$a_2(d_{xy})$	$b_1(d_{zx})$	$2a_1(d_z^2)$	$b_2(d_{yz})$	$1a_1(d_{x^2-y^2})$
$[Cp_2Ti]^{2+}$	−11.45	−11.50	−13.56	−13.97	−15.64
$[Cp_2V]^{2+}$	−10.26	−11.68	−12.80	−11.65	−14.37
$[Cp_2Nb]^{2+}$	−11.24	−11.28	−12.81	−13.58	−15.25
$[Cp_2Mo]^{2+}$	−11.29	−11.30	−13.27	−13.33	−15.09

The variations in the frontier molecular orbital (FMO) energies as a function of the bending angle observed here are very similar to those reported by Lauther and Hoffmann [18] for the bending of normal metallocenes into bent structures. The frontier molecular orbital energies of the bent metallocenes clearly explain the stability and reactivity of the $[Cp_2M]^{2+}$ species (Table 2), considering the FMO energy gap values. The results observed imply that the d^1 electrons of the transition metal systems $[Cp_2V]^{2+}$ and $[Cp_2Nb]^{2+}$ show higher bending than the d^0 $[Cp_2Ti]^{2+}$ and d^2 $[Cp_2Mo]^{2+}$ systems. The order of reactivity is therefore determined by the FMO gap. Among the four bent metallocenes, the $[Cp_2V]^{2+}$ shows the highest reactivity as it has the smallest FMO gap (1.10 eV), while the FMO gaps of $[Cp_2V]^{2+}$ and $[Cp_2Nb]^{2+}$ are low compared to that of $[Cp_2Ti]^{2+}$ due to the availability of a lone nonbonding

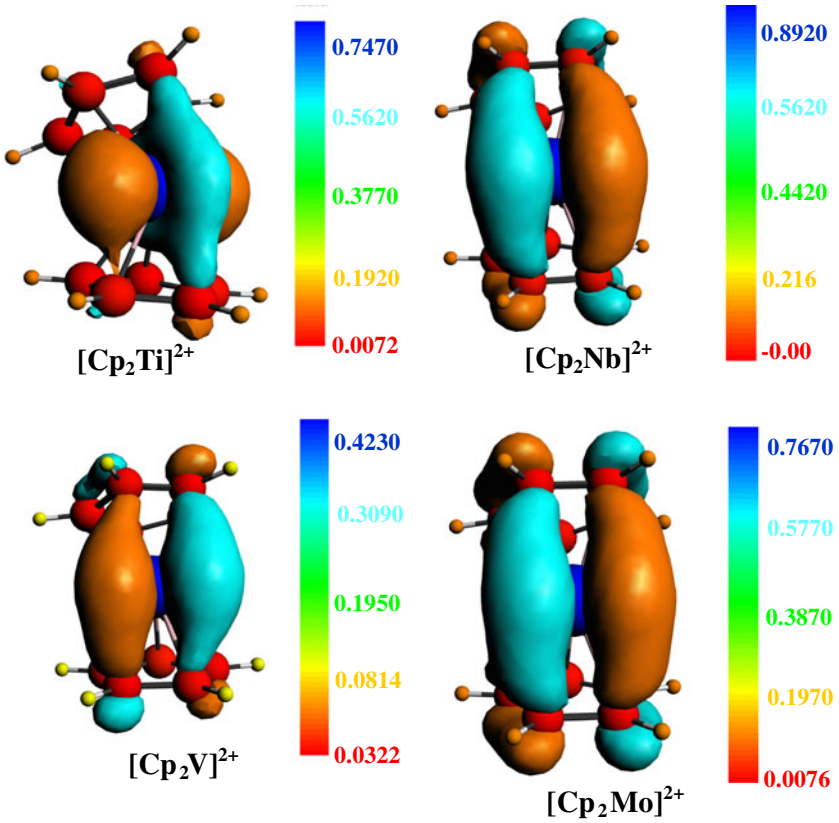

Fig. 2 Hirshfeld charge analysis of various bent metallocene LUMO orbitals

electron (d^1). The FMO gap of $[Cp_2Mo]^{2+}$ is high compared with those of $[Cp_2V]^{2+}$ and $[Cp_2Nb]^{2+}$ due to the availability of lone-pair (d^2) electrons. The four bent metallocenes all have Lewis acidic character since they are electron deficient with respect to the 18-electron rule. In order to explain the Lewis acidic character of the four metallocene species, Hirshfeld charge analysis was carried out (Fig. 2). Hirshfeld charge scanning of the molecular orbitals of bent metallocenes shows that all of the Cp-ring carbons have negative electron density (red color), while the metals have a positive electron density (blue color).

In summary, it is clear that the hydrolyzed forms of $[Cp_2M]^{2+}$ (M = Ti, V, Nb, Mo) species are much more reactive than the corresponding bent metallocene dichlorides, as well as the normal metallocenes. The bending of the $[Cp_2M]^{2+}$ species leads to FMO energy changes, and this is the primary reason for the unusual reactivity of bent metallocenes. The $p(\pi)$–$d(\pi)$ bonding of bent metallocene is directly affected by the bending process, which is evident from the outward bending of the Cp-ring hydrogens. The maximal outward bending value of $[Cp_2Ti]^{2+}$ indicates the maximal $p(\pi)$–$d(\pi)$ overlap between the metal and the Cp ring. The minimal M–Cp ring distances (2.0 Å) also support the above conclusions. The order of reactivity for the $[Cp_2M]^{2+}$ (M = Ti, V, Nb, Mo) species largely depends on the energy gap between the bonding molecular orbital ($2a_1$) and the antibonding molecular orbital (b_1). All of the antitumor-active metallocene species preferentially exist in a bent shape in order to fulfill the octet electron rule, in agreement with previously reported results [29, 30]. The bent shapes of the metallocene species and their resulting Lewis acidic character are important for bent metallocene–nucleotide interactions, and thus for their antitumor drug activities.

Antitumor activity of metallocene dichlorides

To investigate why the bent metallocenes show antitumor activity, four types of bent metallocene–nucleotide adducts were considered—those with adenine, guanine, cytosine, and thymine nucleotides, respectively: Cp_2M(5′-dAMP), Cp_2M(5′-dGMP), Cp_2M(5′-dCMP), and Cp_2M(5′-dTMP) (M = Ti, V, Nb, Mo; see Fig. 3). The X-ray structures of these complexes are known [1].

In the complex, the M(IV) ions are π-bonded to two Cp^- ligands and σ-bonded with one nitrogen atom and one phosphate oxygen atom in the nucleotide unit. All bent metallocenes show high positive charges in their hydrolyzed forms, and in these forms they exhibit Lewis acidic character through empty or partially filled nonbonding orbitals (Fig. 4). The Lewis acidic bent metallocenes

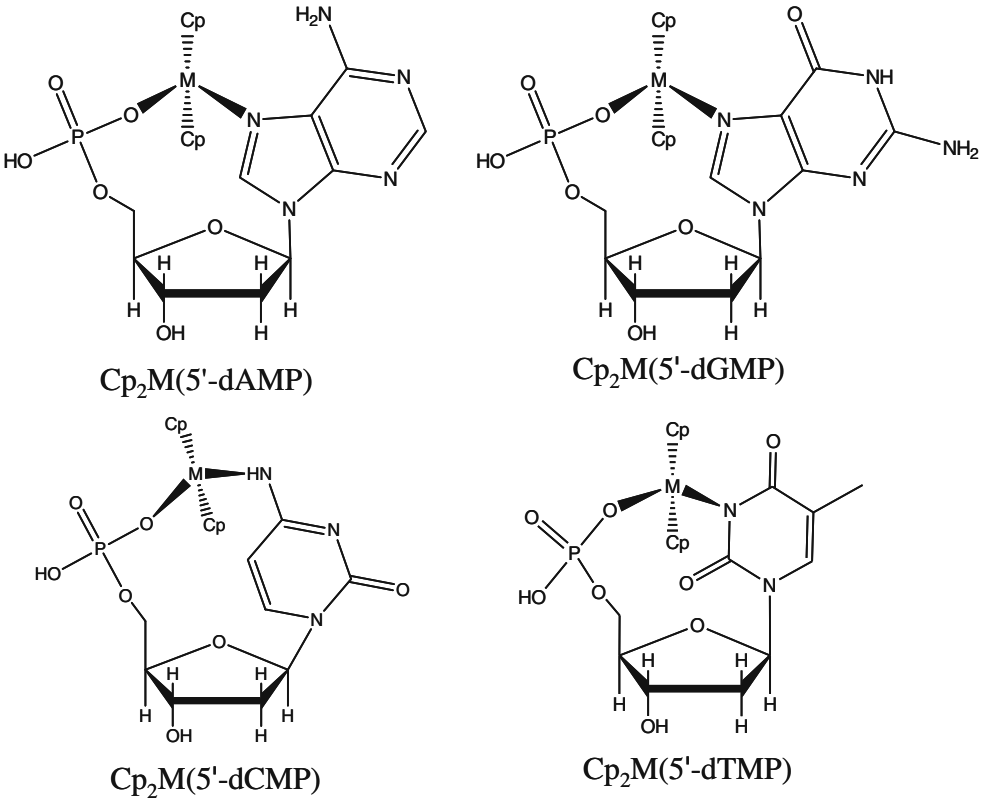

Fig. 3 Bonding modes of bent metallocenes with various nucleotides

interact with nucleobases and with phosphate oxygen through acid–base interactions. Optimized geometries of sixteen bent metallocene–nucleotide complexes are presented in Figs. 5 and 6, and the main bonding parameters are provided in Table 3 along with a reference diagram. The nature of the bonding between the bent metallocenes and the nucleotides and the strengths of these complexes were analyzed by fragment analysis (Table 4). The bent metallocene was considered to be one fragment and the nucleotide part to be another fragment, with no symmetry considerations. The sixteen individual combinations of bent metallocene–nucleotide complexes and the order of their interaction energies are presented in Table 5. In order to explain the nature of the bonding in bent metallocene–nucleotide complexes, the $\Delta E_{elstat}/\Delta E_{orb}$ ratios were calculated, and these are presented in Table 6.

The adenine nucleotide–bent metallocene complexes $Cp_2M(5'\text{-dAMP})$ (M = Ti, V, Nb, Mo) were constructed using available crystallographic information [1]. Geometric optimizations were carried out at the BP86/TZP level. The main optimized geometric parameters of adenine nucleotide–bent metallocene complexes are presented in Table 3. Energy decomposition analysis (EDA) was carried out using the optimized geometries obtained, and the results of this analysis are presented in Table 4. The EDA results for $Cp_2M(5'\text{-dAMP})$ (M = Ti, V, Nb, Mo) adducts show that the order of the interaction energies of the bent metallocene–adenine nucleotide complexes is V > Ti > Nb > Mo. The adenine nucleotide preferentially binds with first-row transition metal metallocenes rather than those of second-row transition metals. Adenine nucleotide–bent metallocene complexes show high $d_{M'-O}$ and $d_{M'-N}$ bond distances for steric reasons. The $Cp_2V(5'\text{-dAMP})$ complex has the strongest interaction energy ΔE_{int} and the largest orbital interaction energy among the four metallocenes. The $Cp_2Ti(5'\text{-dAMP})$ complex has a lower Pauli repulsive interaction ΔE_{Pauli} than $Cp_2V(5'\text{-dAMP})$ due to its d^0 electronic configuration. The lower interaction energy values of the $Cp_2Nb(5'\text{-dAMP})$ and $Cp_2Mo(5'\text{-dAMP})$ complexes indicate that the nonbonding electrons (d^1 and d^2, respectively) repel the incoming ligand. The high ΔE_{int} value of the $Cp_2V(5'\text{-dAMP})$ complex arises because $[Cp_2V]^{2+}$ is the most reactive bent metallocene species; this species readily accepts the N7 lone pair from the adenine base and another two electrons from a phosphate oxygen anion to form a tetrahedral bent metallocene–nucleotide complex.

A similar analysis was performed for the $Cp_2M(5'\text{-dGMP})$ (M = Ti, V, Nb, Mo) adducts. The main structural parameters and energy decomposition analysis results for these species are presented in Tables 3 and 4. The computed values show that the interaction energy ΔE_{int} and the repulsive interaction ΔE_{Pauli} vary for $[Cp_2V]^{2+}$ and $[Cp_2Nb]^{2+}$ in a similar manner to what was seen for the $Cp_2M(5'\text{-dAMP})$ adducts. This is an obvious explanation for the structural similarities of purine-base nucleotides. The interaction energy of $Cp_2V(5'\text{-dGMP})$ is very high

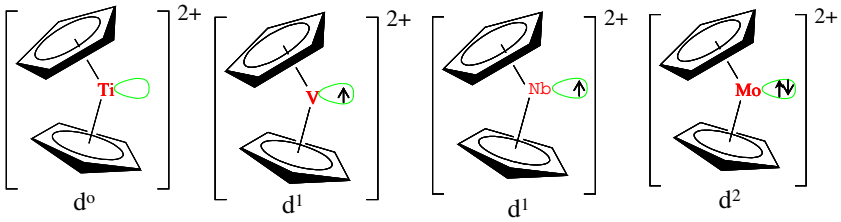

Fig. 4 Bent metallocenes with their nonbonding electrons

compared to those of other adducts due to the higher reactivity and smaller FMO gap of $[Cp_2V]^{2+}$. The high ΔE_{elstat} interaction energy and the low ΔE_{Pauli} repulsive interaction energy of the $Cp_2Ti(5'\text{-dGMP})$ adduct are due to the high positive charge resulting from the empty *d* orbital of $[Cp_2Ti]^{2+}$. In general, the fragment analysis results show that the first-row transition metal (Ti and V) bent metallocenes exhibit the strongest interactions with purine-base (adenine and guanine) nucleotides. The strongest interaction of all occurs between $[Cp_2M]^{2+}$ and guanine nucleotide.

The computed energy decomposition analysis results for $Cp_2M(5'\text{-dCMP})$ and $Cp_2M(5'\text{-dTMP})$ (M = Ti, V, Nb, Mo) adducts are presented in Table 4. These two adducts show

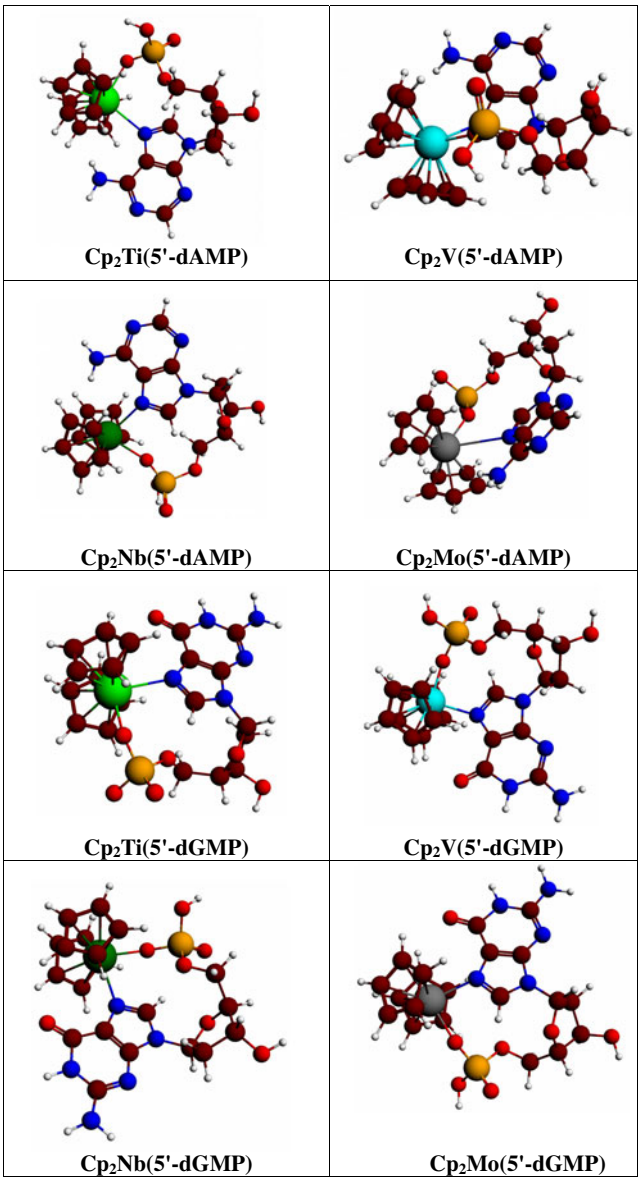

Fig. 5 BP86/TZP-optimized geometries for bent metallocene–purine-base nucleotide complexes

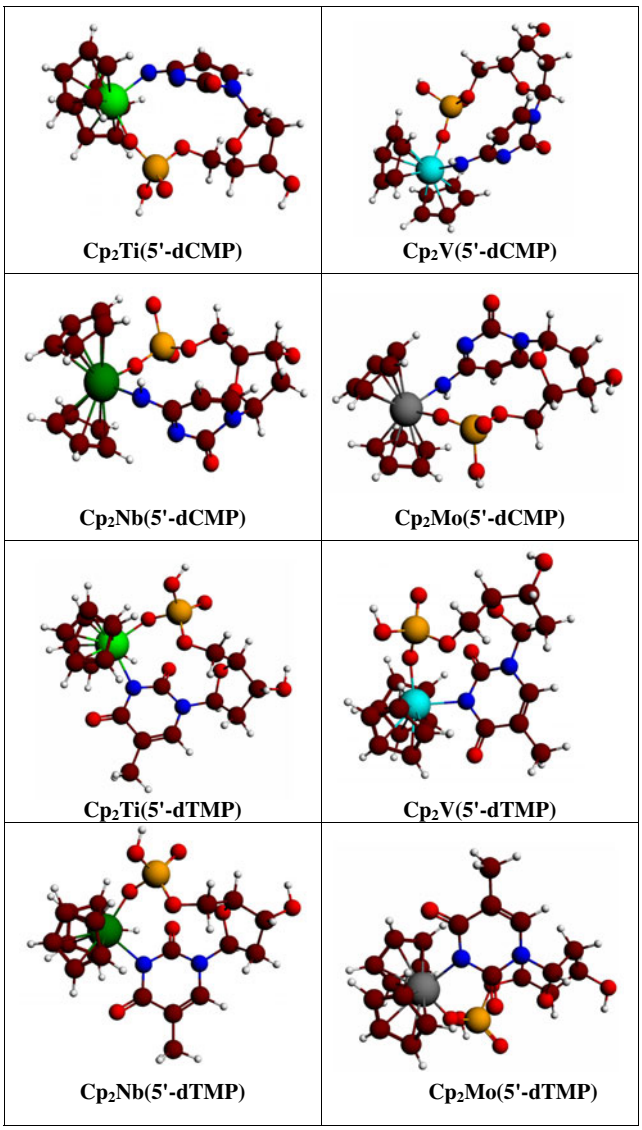

Fig. 6 BP86/TZP-optimized geometries for bent metallocene–pyrimidine-base nucleotide complexes

Table 3 Selected bond parameters for bent metallocene–nucleotide complexes

Type of adducts	γ	φ (Cp-M-Cp)	$d_{Cp'-M}$	θ	$d_{M'-N}$	$d_{M'-O}$
Cp_2Ti(5'-dAMP)	47.8	84.4	2.1	0.2	2.61	2.27
Cp_2Ti(5'-dGMP)	43.4	93.2	2.0	1.1	2.15	2.15
Cp_2Ti(5'-dTMP)	59.0	62.0	2.1	2.7	2.07	1.98
Cp_2Ti(5'-dCMP)	51.3	77.4	2.1	2.3	2.19	1.98
Cp_2V(5'-dAMP)	44.6	90.8	2.0	0.3	2.87	2.03
Cp_2V(5'-dGMP)	43.7	92.6	2.0	3.5	2.37	1.96
Cp_2V(5'-dTMP)	50.0	80.0	1.8	3.8	2.06	2.01
Cp_2V(5'-dCMP)	40.6	100.0	1.8	2.3	2.18	2.03
Cp_2Nb(5'-dAMP)	46.8	86.4	2.1	1.4	2.42	2.28
Cp_2Nb(5'-dGMP)	45.9	88.2	2.0	3.5	2.32	2.14
Cp_2Nb(5'-dTMP)	50.0	80.0	1.8	4.5	2.19	2.04
Cp_2Nb(5'-dCMP)	53.8	72.4	2.2	3.2	2.19	1.98
Cp_2Mo(5'-dAMP)	44.6	90.8	2.0	5.8	2.89	2.19
Cp_2Mo(5'-dGMP)	43.7	92.6	2.0	2.2	2.27	2.20
Cp_2Mo(5'-dGMP)*	(42.0)	(96.1)	(2.0)	-	(2.19)	(2.08)
Cp_2Mo(5'-dTMP)	50.0	100.0	1.8	4.5	2.28	2.19
Cp_2Mo(5'-dCMP)	56.0	68.0	2.2	3.4	2.21	1.97

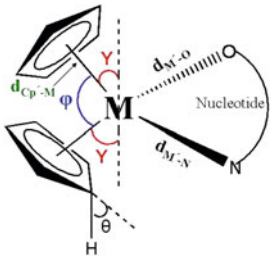

Angle $\gamma\left(\gamma = \frac{180-\varphi}{2}\right)$ and θ in degrees and bond lengths in Å; (*experimental values)[1]

similar trends, and the results indicate that the Cp_2Nb(5′-dCMP) and Cp_2Mo(5′-dCMP) adducts show higher interaction energies than the other two metallocenes, which is because of the increased size of the second-row transition metals and the geometrical effect from the pyrimidine base on the nucleotide.

From an electronic structure perspective, the high ΔE_{int} values of all of the bent metallocene nucleotide complexes indicate that the interactions of the positively charged $[Cp_2M]^{2+}$ species with negatively charged phosphate anionic oxygen and nucleobase nitrogen lone pairs are significant. The bending angle of Cp–M–Cp in the bent metallocene in the complex is larger than that of the free bent metallocene species, which is due to the steric repulsion between the Cp rings and the nucleotide. Generally, in all of the bent metallocene nucleotide complexes, the $d_{M'-O}$ bond is shorter than the $d_{M'-N}$ bond due to the stronger coordination of the phosphate anionic oxygen to the metal than the nucleobase lone-pair electron. One important and interesting observation is the type of bond between the metal part of the metallocene and the nucleotide. The interaction of the positively charged metallocene with the negatively charged nucleotide leads to high ΔE_{int} values, except for molybdocene–nucleotide complexes and the titanocene–thymine nucleotide complex. All of the complexes show higher ΔE_{orb} values than their

Table 4 Energy (kcal mol^{-1}) decomposition analysis of bent metallocene–nucleotide complexes

	Ti				V			
	ΔE_{int}	ΔE_{Pauli}	ΔE_{orb}	ΔE_{elstat}	ΔE_{int}	ΔE_{Pauli}	ΔE_{orb}	ΔE_{elstat}
Cp_2M(5′-dAMP)	−374.15	160.40	−452.46	−82.09	−444.84	365.96	−577.01	−233.80
Cp_2M(5′-dGMP)	−221.26	86.31	−261.19	−46.31	−406.27	183.67	−376.93	−154.34
Cp_2M(5′-dTMP)	−310.73	219.46	−387.31	−142.89	−146.85	387.37	−274.30	−250.93
Cp_2M(5'-dCMP)	−299.18	126.17	−144.12	−155.06	−166.68	293.38	−212.52	−197.55
	Nb				Mo			
Cp_2M(5′-dAMP)	−183.62	150.35	−177.67	−156.30	−197.06	122.42	−151.78	−167.70
Cp_2M(5′-dGMP)	−160.62	161.41	−140.92	−136.11	−136.05	104.87	−110.10	−130.82
Cp_2M(5′-dTMP)	−63.91	137.13	−169.58	−131.45	−227.93	394.42	−229.25	−393.10
Cp_2M(5'-dCMP)	−433.38	73.85	−408.89	−98.85	−401.97	175.34	−419.09	−158.22

Table 5 Trends in the variations of various interaction energy components in bent metallocene–nucleotide complexes at the BP86/TZP level

Energy terms	Cp_2M(5′-dAMP)	Cp_2M(5′-dGMP)	Cp_2M(5′-dTMP)	Cp_2M(5′-dCMP)
ΔE_{int}	V>Ti>Nb>Mo	V>Ti>Nb>Mo	Ti>Mo>V>Nb	Nb>Mo>Ti>V
ΔE_{Pauli}	V>Ti>Nb>Mo	V>Nb>Mo>Ti	Mo>V>Ti>Nb	V>Mo>Ti>Nb
ΔE_{elstat}	V>Ti>Nb>Mo	V>Ti>Nb>Mo	Ti>V>Mo>Nb	Mo>Nb>V>Ti
ΔE_{orb}	V>Mo>Nb>Ti	V>Nb>Mo>Ti	Mo>V>Ti>Nb	V>Nb>Ti>Mo
$\Delta E_{elstat}/\Delta E_{orb}$	Mo>Nb>V>Ti	Mo>Nb>V>Ti	Mo>V>Nb>Ti	Ti>V>Mo>Nb

ΔE_{int} values. The orbital contribution plays a vital role in bent metallocene–nucleotide complex formation. According to the molecular orbital energy levels of the bent metallocene and the symmetry requirements for σ bonding, $2a_1$ and b_2 would be involved in σ-bond formation. The anionic oxygen of the phosphate unit and the lone pair of the nucleobase nitrogen can easily approach the metal's $2a_1$and b_2 orbitals with appropriate symmetry. This is why the ΔE_{orb} values are higher than the ΔE_{int} values. Except for the Cp_2Mo(5′-dCMP) complex, all of the molybdocene–nucleotide complexes show quite high ΔE_{elstat} values due to the repulsion between the a_2 molecular orbital lone pair and the incoming nucleotide part. The $\Delta E_{elstat}/\Delta E_{orb}$ ratio values (Table 5) clearly explain the character of the bonding between the bent metallocene species and the nucleotides. Except for molybdocene–nucleotide complexes and Cp_2Ti (5′-dCMP), all of the $\Delta E_{elstat}/\Delta E_{orb}$ ratios are less than one, and this highlights the nature of the bonding in nucleotide–bent metallocene complexes. The tabulated values (Table 6) show that the bonds between the nucleotides and bent metallocenes are preferentially covalent rather than ionic.

Bent metallocene dichlorides hydrolyze under physiological conditions to give $[Cp_2M]^{2+}$ species that inhibit DNA through coordination. The high negative values of ΔE_{int} seen for all sixteen bent metallocene–nucleotide complexes clearly explain the coordination of bent metallocene with DNA, and they agree very well with previously reported results. Among the metallocenes considered here, $[Cp_2Ti]^{2+}$ and $[Cp_2V]^{2+}$ exhibit stronger interactions with purine-base nucleotides, and $[Cp_2V]^{2+}$ is very reactive species that shows stronger interactions with all of the nucleotides than $[Cp_2Ti]^{2+}$. Among the four nucleobases, the purine-base nucleotides interact effectively with first-row bent metallocene species due to geometric factors and N7 lone-pair availability. The $\Delta E_{elstat}/\Delta E_{orb}$ values explain the covalent nature of the bent metallocene–nucleotide complexes. The pyrimidine–base nucleotides preferably interact with second-row transition metal-containing metallocenes, and this leads to higher interaction energy values. From an electronic structure perspective, the $2a_1$ and b_2 MOs of bent metallocenes are involved in σ-bond formation, and the energy gap between these two MOs determines the reactivity of the $[Cp_2M]^{2+}$ species. The interaction of the bent metallocene with the nucleotide is dictated by the electronic structure of the active bent metallocene species.

Table 6 $\Delta E_{elstat}/\Delta E_{orb}$ values of bent metallocene–nucleotide complexes

	Ti	V	Nb	Mo
Cp_2M(5′-d AMP)	0.18	0.41	0.87	1.10
Cp_2M(5′-d GMP)	0.17	0.40	0.96	1.18
Cp_2M(5′-d TMP)	0.36	0.91	0.77	1.71
Cp_2M(5′-d CMP)	1.01	0.92	0.24	0.37

Summary and conclusions

Density-functional calculations at the BP86 level have been carried out on a series of experimentally characterized bent metallocene–nucleotide adducts to gain insights into the unusual reactivities of bent metallocenes and their antitumor activities. In order to understand the orbital electronic structures of free bent metallocene ions, electronic structure analysis and Walsh energy analysis have been carried out on the optimized bent metallocene geometries. The hydrolyzed form of the bent metallocene dichloride $[Cp_2M]^{2+}$ is involved in complex formation with nucleotides. The bent metallocenes also coordinate with incoming ligands in order to fulfill the 18-electron rule. The bending process reduces symmetry, resulting in the splitting of five molecular orbital levels. During the bending process, the energy of the bonding molecular orbital ($2a_1$) increases while the energy of the antibonding molecular orbital (b_1) drops, decreasing the energy gap. The reduced energy gap between these two orbitals is responsible for the high reactivities of the bent metallocene species. According to the FMO gap, the order of reactivity of the four bent metallocenes is: $[Cp_2V]^{2+} > [Cp_2Nb]^{2+} > [Cp_2Mo]^{2+} > [Cp_2Ti]^{2+}$.

When bending is minimized, a higher $p(\pi)$–$d(\pi)$ overlap results, and this in turn maximizes the outward bending of the Cp-ring hydrogens. Based on the computed outward bending values, titanocene and molybdocene show higher $p(\pi)$–$d(\pi)$ overlaps than the other two metallocenes. Minimizing the bending also results in greater outward

bending of the ring hydrogens. Among the four bent metallocenes considered here, $[Cp_2Ti]^{2+}$ shows the smallest bending angle Y and the largest $p(\pi)$–$d(\pi)$ overlap.

Energy decomposition analysis of the nucleotide–bent metallocene complexes suggests that the positively charged bent metallocenes accommodate two pairs of electrons when they bond with nucleotides, and that the metal center assumes the T_d shape. The high interaction energies ΔE_{int} of all sixteen nucleotide–bent metallocene complexes explain their coordination, and correlate well with their comparative antitumor activities. Based on the ΔE_{int} values, $[Cp_2V]^{2+}$ shows the strongest interactions with all of the nucleotides, and the purine-base nucleotides show preferential coordination with first-row transition metal-containing metallocenes. The pyrimidine-base nucleotides prefer to interact with second-row transition metal-containing bent metallocenes. The $\Delta E_{elstat}/\Delta E_{orb}$ ratios clearly show that there is a covalent bond between the bent metallocene and the nucleotide.

Acknowledgments We thank the Council of Scientific and Industrial Research, India, for their financial support in the form of a research grant (Ref. No. 02(2158)/07/EMR-II). DS thanks the Council of Scientific and Industrial Research for financial support through a Senior Research Fellowship. Support from the Indian National Science Academy and the German Research Foundation (DFG) in the form of an exchange visit to Marburg in 2003 is gratefully acknowledged by PV.

References

1. Kuo LY, Mercouri G, Kanatzidis MG, Sabat M, Tipton AL, Marks TJ (1991) J Am Chem Soc 113:9027–9045
2. Rosenberg B (1985) Cancer 55:2303–2316
3. Köpf-Maier P, Köpf H (1988) Struct Bond 70:105–185 (and references therein)
4. Köpf-Maier P, Köpf H (1986) Drugs Future 11:297–319 (and references therein)
5. Köpf-Maier P, Moormann A, Köpf H (1985) Eur J Cancer Clin Oncol 21:853–857
6. Köpf-Maier P, Wagner W, Köpf H (1981) Cancer Chemother Pharmacol 5:237–241
7. Köpf-Maier P, Wagner W, Hesse B, Voigtlander R, Köpf H (1980) J Cancer Res Clin Oncol 97:31–39
8. Köpf-Maier P, Wagner W, Köpf H (1980) J Cancer Res Clin Oncol 96:43–51
9. Köpf H, Köpf-Maier P (1979) Angew Chem Int Ed Engl 18:477–487
10. Köpf-Maier P, Köpf H (1988) J Organomet Chem 342:167–176
11. Murthy M, Toney JH, Rao LN, Marks TJ (1986) Proc Am Assoc Cancer Res 27:279
12. Toney JH, Rao LN, Murthy MS, Marks TJ (1985) Breast Cancer Res Treat 6:185
13. Murthy MS, Rao LN, Kuo LY, Toney JH, Marks TJ (1988) Inorg Chim Acta 152:117–124
14. Bruhn SL, Toney JH, Lippard GJ (1990) Prog Inorg Chem 38:477–516
15. Lippert B (1989) Prog Inorg Chem 37:1–97
16. Reedijk J, Fichtinger-Schepman AMJ, van Oosterom AT, van do Putte P (1987) Struct Bond (Berlin) 67:1153–1181
17. Sherman SE, Lippert SJ (1987) Chem Rev 87:1153–1181
18. Barnard CFJ, Cleare MJ, Hydes PC (1986) Chem Brit 22:1001–1004
19. Köpf-Maier P, Wagner W, Köpf H (1981) Naturwissenschaften 68:272–273
20. Köpf- Maier P, Köpf H (1980) Naturwissenschaften 67:415–416
21. Berdel WE, Schmoll HJ, Scheulen ME, Korfel A, Knoche MF, Harstrick A, Bach F, Baugmart J, Saβ G (1993) Onkologie 16: R172
22. Harding MM, Mokdsi G (2007) Curr Med Chem 7:1289–1303
23. Yan YK, Melchart M, Heptemariam A, Sedler PJ (2005) Chem Commun 4764–4776
24. Korfel A, Scheulen ME, Schmoll HJ, Gründel O, Harstrick A, Knoche M, Fels LM, Skorzec M, Bach F, Baumgart J, Saβ G, Seeber S, Thiel E, Berdel WE (1998) Clin Cancer Res 4:2701–2708
25. Christodoulou CV, Ferry DR, Fyfe DW, Young A, Doran J, Scheehan TMT, Eliopoulos A, Hale K, Baumgart J, Saβ G, Kerr DJ (1998) J Clin Oncol 16:2761–2769
26. Lümmen M, Sperling S, Luboldt H, Otto T, Rübben H (1998) Cancer Chemother Pharmacol 42:415–417
27. Kröger N, Kleeberg UR, Mross K, Edler L, Saβ G, Hossfeld (2000) Onkologie 23:60–62
28. Osmond J, D'Cruz OJ, Ghosh P, Uckun FM (1998) Biol Reprod 58:1515–1526
29. Joseph WL, Hoffmann R (1976) J Am Chem Soc 98:1729–1742
30. Clarke MJ, Zhu F, Frasca DR (1999) Chem Rev 99:2511–2534
31. Retting MF (1974) Review of molecular orbital calculations for metallocenes. In: LaMar GN, DeW W, Horrocks Jr, Holm RH (eds) NMR of paramagnetic molecules: principles and applications. Academic, New York
32. Ashley AE, Cooper RT, Wildgoose GG, Green JC, O'Hare D (2008) J Am Chem Soc 130:15662–15677
33. Sobota P, Dra-g-Jarza-bek A, John Y, ozef Utko J, Jerzykiewicz LB, Duczmal M (2009) Inorg Chem 48:6584–6593
34. Doman TN, Landis CR, Bosnich B (1992) J Am Chem Soc 114:7264–7212
35. Bercaw JE, Resenberg E, Roberts JD (1974) J Am Chem Soc 96:612–614
36. te Velde G, Bickelhaupt F, Baerends EJ, van Gisbergen SAJ, Fonseca GC, Snijders JG, Ziegler T (2001) J Comput Chem 22:931–967
37. Guerra CF, Snijders JG, te Velde G, Baerends EJ (1998) J Theor Chem Acc 99:391–403
38. Scientific Computing & Modelling NM (2010) Amsterdam density functional. Scientific Computing & Modelling NV, Amsterdam (http://www.scm.com)
39. Perdew JP, Burke K, Ernzerhof M (1996) Phys Rev Lett 77:3865–3868
40. van Lenthe E, Baerends EJ, Snijders JG (1993) J Chem Phys 99:4597–4610
41. van Lenthe E, Baerends EJ, Snijders JG (1994) J Chem Phys 101:9783–9792
42. van Lenthe E, Ehlers AE, Baerends EJ (1999) J Chem Phys 110:8943–8953
43. Morokuma K (1971) J Chem Phys 55:1236–1244
44. Ziegler T, Rauk A (1977) Theor Chim Acta 46:1–10
45. Esterhuysen C, Frenking G (2004) Theor Chem Acc 111:381–389

46. Krapp A, Bickelhaupt FM, Frenking G (2006) Chem Eur J 12:9196–9216
47. Frenking G, Solà M, Vyboishchikov SF (2005) J Organomet Chem 690:6178–6204
48. Frenking G, Wichmann K, Fröhlich N, Loschen C, Lein M, Frunzke J, Rayón VM (2003) Coord Chem Rev 55:238–239
49. Lein M, Frenking G, Dykstra CE, Kim KS, Scuseria GE (2005) Chapter 13. In: Theory and applications of computational chemistry: the first 40 years. Elsevier, Amsterdam
50. Rayón VM, Frenking G (2003) Organometallics 22:3304–3308
51. Lein M, Frunzke J, Frenking G (2003) Inorg Chem 42:2504–2511
52. Jemmis ED, Alexandratos S, Schleyer PVR, Streitwieser AJ III, Schaefer HF (1978) J Am Chem Soc 100:5695–5700